

---

**Archiv-Ex.:**

FZR-95

June 1995

Preprint

*L. Käubler, J. Döring, L. Funke, P. Kleinwächter,  
H. Prade, J. Reif, R. Schwengner, G. Winter,  
I.N. Vishnevski, M.J. Kirichenko, Yu.N. Lobach,  
I.P. Tkachuk, V.V. Trishin, M.F. Kudojarov, E.V. Kusmin,  
A.A. Pasternak, J. Blomqvist and L. Kostova*

**In-Beam Investigation  
and the Structure of States in  $^{113}\text{Sn}$**

**Forschungszentrum Rossendorf e.V.**

Postfach 51 01 19 · D-01314 Dresden

Bundesrepublik Deutschland

Telefon (0351) 591 3589

Telefax (0351) 591 3700

E-Mail [kaeubler@fz-rossendorf.de](mailto:kaeubler@fz-rossendorf.de)

# In-Beam Investigation and the Structure of States in $^{113}\text{Sn}$

L. Käubler<sup>1</sup>, J. Döring<sup>8</sup>, L. Funke<sup>7</sup>, P. Kleinwächter<sup>2</sup>, H. Prade<sup>2</sup>, J. Reif<sup>2</sup>, R. Schwengner<sup>2</sup>, G. Winter<sup>2</sup>, I.N. Vishnevski<sup>3</sup>, M.J. Kirichenko<sup>3</sup>, Yu.N. Lobach<sup>3</sup>, I.P. Tkachuk<sup>3</sup>, V.V. Trishin<sup>3</sup>, M.F. Kudojarov<sup>4</sup>, E.V. Kusmin<sup>4</sup>, A.A. Pasternak<sup>4</sup>, J. Blomqvist<sup>5</sup> and L. Kostova<sup>6</sup>

<sup>1</sup> Technische Universität Dresden, Institut für Kern- und Teilchenphysik, Mommsenstr. 13, D-01062 Dresden, Germany (e-mail: kaeubler@fz-rossendorf.de)

<sup>2</sup> FZ Rossendorf, Institut für Kern- und Hadronenphysik, Postfach 510119, D-01314 Dresden, Germany

<sup>3</sup> Institute for Nuclear Research of the Ukrainian Academy of Science, Prospekt Nauki, 252028 Kiev, Ukraine

<sup>4</sup> Physico-Technical Institute "A.F. Joffe", Cyclotron Laboratory, Ul. Politechnitscheskaja 26, 194021 St.Petersburg, Russia

<sup>5</sup> Royal Institute of Technology, Physics Department, Frescati, Frescativägen 24, S-10405 Stockholm, Sweden

<sup>6</sup> Institute for Nuclear Research and Nuclear Energy, Bulgarian Academy of Sciences, Tzarigrad Chaussee 72, BG-1784 Sofia, Bulgaria

<sup>7</sup> Ingenieurgesellschaft IAF, Karpatenstr. 20, D-01326 Dresden, Germany

<sup>8</sup> Department of Physics, Florida State University, Tallahassee, Florida 32306-3016, U.S.A.

## Abstract

The results of in-beam investigations of  $^{113}\text{Sn}$  using the  $(p,n)$ ,  $(p,3n)$ ,  $(\alpha,n)$  and  $(\alpha,2n)$  reactions are summarized. Excited states have been identified until  $E_x = 4715$  MeV and  $J^\pi = (27/2^-)$ . For a large number of levels mean lifetimes  $\tau$  have been determined with the DSA method. For the  $J^\pi = 25/2^+$  state at  $E_x = 4059$  MeV,  $\tau = 1.0(4)$  ns has been measured with the  $\gamma$ -RF method. The experimental results are compared with the predictions of shell-model calculations. Most of the positive-parity states may be considered as one- or three-quasiparticle neutron excitations of the  $2d_{5/2}$ ,  $1g_{7/2}$ ,  $3s_{1/2}$  and  $2d_{3/2}$  shells, the negative-parity states as the coupling of one  $1h_{11/2}$  neutron to the two- or four-quasiparticle neutron excitations in the even-mass  $^{112}\text{Sn}$  core. For the  $25/2^+$  isomer the three-quasiparticle neutron configuration  $\nu(h_{11/2}^2 g_{7/2}^{-1})$  has been proposed on the basis of a shell-model analysis using the mass formula formalism. The experimentally observed yrast states in  $^{113}_{50}\text{Sn}_{63}$  are compared with the corresponding states in the valence-mirror nucleus  $^{145}_{63}\text{Eu}_{82}$  giving remarkable similarities although the parameters for the shell-model calculations differ considerably. The analysis of nearest-neighbour spacing distributions of  $5/2^+$  states in  $^{113}\text{Sn}$  does not allow definite conclusions about regularity or chaos.

## 1 Introduction

At present the semi magic  $Z = 50$  tin nuclei with  $N \leq 64$  are investigated very intensively [1–10]. Generally, the tin nuclei offer the possibility to investigate the nuclear structure of one element for a large variation of the neutron number  $N$ , namely for  $50 \leq N \leq 82$  from  $^{100}\text{Sn}$  to  $^{132}\text{Sn}$ . Nowadays, mainly efficient gamma arrays, e.g. OSIRIS, EUROGAM, NORDBALL and GAMMASPHERE, and heavy-ion reactions are used to investigate high-spin states at high excitation energy or to identify states in nuclei, which are produced with very small cross sections. Nevertheless, the detailed investigation of low-lying states with medium spins remains an interesting task. These states are important to fix the Hamilto-

nian's of nuclear structure models.

In the tin nuclei with  $N \leq 64$  a large variety of different nuclear excitation modes has been found. Besides spherical many-quasiparticle excitations of the  $N = 50$  neutrons in the  $1g_{7/2}$ ,  $2d_{5/2}$ ,  $3s_{1/2}$ ,  $2d_{3/2}$  and  $1h_{11/2}$  shell-model orbits [11–13], also vibrational states [14] and deformed rotational states [1, 2, 10, 15–19] assuming the alignment of neutrons in the  $1h_{11/2}$  orbit or the break-up of the  $Z = 50$  proton core have been observed.

The present paper is a compilation of results for  $^{113}\text{Sn}$  which have been partly published elsewhere [20–32]. In comparison with the experimental data of  $^{113}\text{Sn}$  known from the compilation [33], in the present paper a large amount of new positive- and negative-parity states is presented, which are partly also contained in [34]. The structure of the experimentally observed states in  $^{113}\text{Sn}$  is discussed in the framework of the spherical shell model. The comparison of valence neutrons and protons outside the magic  $N, Z = 50$  and  $N = 82$  cores in the  $Z = 50$  nucleus  $^{113}\text{Sn}$  and the  $N = 82$  nucleus  $^{154}\text{Eu}$  using the concept of quasi-mirror nuclei [13], lateron called valence mirror nuclei [35–37], allows the consideration of symmetry aspects of nuclear systems with the same number of active neutrons and protons. Furtheron, the available target materials to investigate  $^{113}\text{Sn}$  give the opportunity to excite states by different types of reactions and, therefore, to identify all existing levels in a certain range of excitation energy in the sense of complete spectroscopy. The nucleus  $^{116}\text{Sn}$  is one of the few examples in the whole chart of nuclides investigated in this manner [38]. Further experimental data are needed to decide the question whether the nucleons are behaving chaotic or not. Here the nearest-neighbour spacing distributions of  $5/2^+$  states are discussed.

## 2 Experimental procedure and results

The experimental results have been obtained in a Kiev(K)-Petersburg(P)-Rossendorf(R) collaboration. Using the proton or alpha particle induced reactions (p,n), (p,3n), ( $\alpha$ ,n) and ( $\alpha$ ,2n) with particle energies of  $E_p = 6.7$ ,  $E_p = 30$ ,  $E_\alpha = 18$  and  $E_\alpha = 27$  MeV, respectively, singles  $\gamma$ -ray spectra (K,P), angular distributions (K), Doppler-shift attenuation spectra (P),  $\gamma$ -linear polarization spectra and  $\gamma$ -RF time distributions (R), and coincidence spectra (K) have been measured.

Details to the measurement of excitation functions, angular distributions and coincidences using the (p,n) and (p,3n) reactions are given in [23] and [24]. Thereby, targets of a thickness of  $7 \text{ mg/cm}^2$  enriched to 87 % and 99,9 % for  $^{113}\text{In}$  and  $^{115}\text{In}$ , respectively, have been used. In [27] the determination of relative gamma-ray intensities,  $A_2$  and  $A_4$  values using the reactions  $^{110}\text{Cd}(\alpha,n)$  and  $^{111}\text{Cd}(\alpha,2n)$  is described. There also a description of the determination of lifetimes in the ps-region by means of the Doppler-shift attenuation method in the ( $\alpha$ ,n) reaction is given, where a  $14 \text{ mg/cm}^2$  thick metallic  $^{110}\text{Cd}$  target has been used.

The linear polarization of  $\gamma$ -rays has been measured with a planar Ge(Li) detector having a geometrical size of  $27 \times 27 \times 5 \text{ mm}^3$ . This Compton polarimeter has been arranged parallel or perpendicular to the beam axis by means of a turn-table in a two hours cycle. The distance between the target center and the detector surface amounted to 72 mm. The reaction  $^{111}\text{Cd}(\alpha,2n)^{113}\text{Sn}$  has been used bombarding a  $21 \text{ mg/cm}^2$  thick metallic  $^{111}\text{Cd}$  target with 27 MeV  $\alpha$ -particles. The measuring time for each detector position amounted to 24 h. The procedure to obtain the experimental polarization  $P_{exp}$  is described in more detail in [39]. The conservation or the change of parity between the initial and final state of a  $\gamma$ -transition is obtained by the comparison of  $P_{exp}$  with the polarization  $P_{a.d.}$  calculated with the experimentally determined angular distribution coefficients  $A_2$  and  $A_4$ .

With the same target, reaction and beam energy,  $\gamma$ -RF time distributions [40, 41] have

been measured to obtain lifetimes of levels in the ns-region. Thereby a true coaxial Ge(Li) detector was positioned at  $55^\circ$  relative to the beam axis. By means of the centroids of background corrected time distributions of prompt  $\gamma$ -transitions a prompt reference curve was determined. The difference between the centroid of a delayed transition and the centroid of the prompt reference curve at the same  $\gamma$ -ray energy gives directly the mean lifetime  $\tau$  of the deexciting level under the assumption, that the initial state is not fed by a delayed transition.

The data obtained in the experiments mentioned above are summarized in Table 1 and in the level scheme of  $^{113}\text{Sn}$  shown in Fig. 1 and Fig. 2. The level scheme has been constructed on the basis of the  $\gamma$ -ray energies, the relative intensities of the  $\gamma$ -transitions, the excitation functions of the  $\gamma$ -rays, the coincidence relations, the lifetimes of the states in the ps- and ns- regions, the angular distribution coefficients and the corresponding attenuation factors [42], the mixing ratios and the linear polarization of  $\gamma$ -rays. In comparison with [33] a large number of new transitions has been observed and many new states have been identified.

### 3 A shell-model interpretation of $^{113}\text{Sn}$

In a discussion of the structure of states in  $^{111}\text{Sn}$  we presented a Hamiltonian for shell-model calculations for tin nuclei [13] with  $N \leq 64$ . In the following the results of calculations for  $^{113}\text{Sn}$  are given using the same shell-model parameters.

#### 3.1 Positive-parity states

For the calculations with the spherical shell model with configuration mixing (SMC) the doubly magic  $N = Z = 50$  core is assumed. The remaining 13 valence neutrons are distributed over the  $2d_{5/2}$ ,  $1g_{7/2}$ ,  $3s_{1/2}$  and  $2d_{3/2}$  shells forming the configurations  $(g_{7/2}, d_{5/2})^{13}$  and  $(g_{7/2}, d_{5/2})^{12} (s_{1/2}, d_{3/2})^1$ . For the two-body part of the Hamiltonian, the surface delta interaction (SDI) with  $A = 0.479$  MeV has been applied and the single-particle energies  $\varepsilon_{d_{5/2}} = 0$  MeV,  $\varepsilon_{g_{7/2}} = 0.32$  MeV,  $\varepsilon_{s_{1/2}} = 2.57$  MeV and  $\varepsilon_{d_{3/2}} = 3.07$  MeV have been used. The theoretical results for  $^{113}\text{Sn}$  are compared with the experimentally observed positive-parity states in Fig. 3.

The excitation energy of the states with  $E_x < 0.5$  MeV is predicted quite well. The corresponding wave functions contain predominantly single-particle contributions. All calculated levels with higher excitation energy are seniority  $\nu = 3$  states with the configurations  $(g_{7/2}, d_{5/2}, s_{1/2})^3$  or  $(g_{7/2}, d_{5/2}, d_{3/2})^3$ . They are predicted at an about 1 MeV too high excitation energy. This energy shift is mainly caused by the restrictions of the shell-model space in our calculations. Calculations within larger configuration spaces, e.g. our large scale shell-model calculation for  $^{109}\text{Sn}$  [9, 43], the large scale shell-model calculations of Ogawa and Momoki, cited in [6], of Engeland [44] and of Schubart et al. [5] as well as the quasiparticle multistep shell-model calculations of Sandulescu et al. [45] for different tin nuclei with  $N < 64$  give the three-quasiparticle states at about the experimentally observed excitation energies. Despite the energy shift the restrictions of the configuration space in our calculations seem to be appropriate for the experimentally observed positive-parity states with  $E_x < 3$  MeV. Levels with more than three excited particles in the  $1g_{7/2}$ ,  $2d_{5/2}$ ,  $2d_{3/2}$  and  $3s_{1/2}$  shells have been found both in the experiments to  $^{105}\text{Sn}$  [5],  $^{107}\text{Sn}$  [6] and  $^{109}\text{Sn}$  [9], and in the calculations mentioned above at excitation energies  $E_x > 3$  MeV.

As shown in Fig. 3, the experimentally observed level density for states with  $E_x > 1$  MeV is reproduced by the calculations. Going into more detail, in Fig. 4 all measured and calculated three-particle states with a spin and parity assignment of  $3/2^+ \leq J^\pi \leq 7/2^+$  are

compared. In the experiments 22 states have been found, the calculations give 23 states. In conclusion, the experimentally observed low-spin positive-parity states are seniority  $\nu = 1$  or  $\nu = 3$  neutron excitations and for states with  $E_x < 3$  MeV the number of experimentally observed levels corresponds nearly to the number of theoretical predicted states.

### 3.2 Negative-parity states

As for  $^{111}\text{Sn}$  [13], we performed also particle-core coupling (PCC) calculations for the interpretation of negative-parity states in  $^{113}\text{Sn}$ , coupling one  $1h_{11/2}$  neutron to a truncated number of positive-parity shell-model states in the core  $^{112}\text{Sn}$ . The model is described in [46]. Thereby, from the  $^{112}\text{Sn}$  core states which have been calculated with the same shell-model parameters as mentioned in Subsection 3.1, all yrast states and all states with  $E_x < 3.5$  MeV have been selected. The single-particle energy  $\varepsilon_{h_{11/2}} = 3.33$  MeV has been used. In Fig. 5 the calculated level energies are compared with the experimental findings, where the experimentally observed and calculated yrast states are connected by lines. Considering the wave functions, most of the calculated states which are predicted at too high excitation energy, e.g. the  $9/2^-$ ,  $13/2^-$  and  $15/2^-$  yrast states (dashed lines), have large contributions of couplings of the  $1h_{11/2}$  neutron to the  $2_1^+$  core state in  $^{112}\text{Sn}$ . The levels which are calculated too low in comparison to the experiments, e.g. the  $17/2^-$ ,  $19/2^-$ ,  $21/2^-$  and  $23/2^-$  yrast states (dashed-dotted lines), are mainly formed by the coupling to the  $4_1^+$  and  $6_1^+$  core states. These energy shifts observed in the PCC calculations for  $^{113}\text{Sn}$  are caused by the position of the calculated  $0_1^+$ ,  $2_1^+$ ,  $4_1^+$  and  $6_1^+$  states in  $^{112}\text{Sn}$  which are dominating excitations of two neutrons to the  $2d_{5/2}$  and  $1g_{7/2}$  shells. As shown in Fig. 6, the  $2_1^+$  state is predicted too high, the  $4_1^+$  and  $6_1^+$  state too low. Despite the energy shifts, the calculations for  $\pi = -1$  states in  $^{113}\text{Sn}$  give a level density similar to the experiments. As a result of the PCC calculations, most of the observed negative-parity states in  $^{113}\text{Sn}$  with  $9/2^- \leq J^\pi \leq 23/2^-$  are three-quasiparticle states, where one  $1h_{11/2}$  neutron couples dominantly to the  $0^+ \leq J^\pi \leq 6^+$  states of the  $^{112}\text{Sn}$  core.

The experimentally observed  $0_1^+$ ,  $2_1^+$ ,  $4_1^+$  level distances in  $^{112}\text{Sn}$  (Fig. 6) show vibrational-like behaviour in accordance with [14], whereas the SMC calculations give typical spherical shell-model multiplet states. This is a general feature of shell-model calculations for even-mass tin nuclei with  $A \leq 114$  which allow only neutron excitations. Thus, the quasiparticle multistep shell-model calculations [45] mentioned in Subsect. 3.1, where also the SDI is used to calculate the two-body matrix elements give for  $^{112}\text{Sn}$   $0_1^+ - 2_1^+ - 4_1^+$  distances near to the experiments but the  $4_1^+ - 6_1^+$  energy difference is predicted by a factor of about 2 too large. Large scale shell-model calculations [48] to  $^{114}\text{Sn}$  overestimate the excitation energy of the  $2_1^+$  state but give too small excitation energies of the  $4_1^+$  and  $6_1^+$  levels. As a further example, the large scale shell-model calculations [44] for  $^{110}\text{Sn}$  using realistic effective interactions can be compared with our predictions for  $^{110}\text{Sn}$ , calculated within the same restricted model space as for  $^{112}\text{Sn}$  and  $^{113}\text{Sn}$ . The large scale shell model calculations give for  $^{110}\text{Sn}$  the  $0_1^+ - 2_1^+$  distance near to the experiment. The excitation energies of the  $4_1^+$  and  $6_1^+$  states are nearly the same as in our restricted calculations to  $^{110}\text{Sn}$ , i.e. too small compared to the experiment. In conclusion, by means of larger configuration spaces and more realistic effective interactions, the  $0_1^+ - 2_1^+$  level distance in the even tin nuclei with  $N < 64$  is better reproduced than in our restricted calculations, but the general difficulties to reproduce the distances of low-lying levels in tin nuclei are not removed.

### 3.3 Electromagnetic properties

The wave functions obtained within the SMC and PCC calculations have been used to calculate electromagnetic properties. In Table 2 the available experimentally obtained reduced transition probabilities  $B(\sigma L)$ , as well as magnetic and quadrupole moments for yrast states in  $^{113}\text{Sn}$  are compared with the corresponding theoretical predictions.

The calculated  $B(\sigma L)$  values are in most cases smaller than the experimental results. With the exception of the E3 contribution to the  $11/2^- \rightarrow 7/2^+$  transition, and of the  $17/2^- \rightarrow 13/2^-$  E2 transition, the predicted  $B(\sigma L)$  values deviate by factors of about  $10^{-5}$  to 4 from the experimental ones. The calculations give for the magnetic moments nearly the single-particle values renormalized by  $g_s^{eff} = 0.6g_s^{free}$ . The calculations of the electromagnetic properties show that the wave functions contain possibly too few components which allow electromagnetic transitions. As a conclusion, the shell model space used has to be enlarged to get more appropriately calculated electromagnetic properties. Once more, only the comparison of measured and calculated electromagnetic properties allows serious conclusions on whether a nuclear structure model is adequate to the experimental observations or not.

## 4 The $\nu(h_{11/2}^2 g_{7/2}^{-1})$ structure of the $25/2^+$ isomer

As shown in Fig. 1 a ns-isomer at  $E_x = 4059.1$  keV could be identified in this work. In comparison with [10] the spin and parity of the levels above the 3129.9 keV state could be determined unambiguously and the sequence of the 291.7 and 551.9 keV transitions has been changed. Because of the E1-character of the 599.5 keV transition, we could ascribe  $J^\pi = 25/2^+$  to the level at 4059.1 keV. Additionally, for this state a half-life of  $T_{1/2} = 0.7(3)$  ns has been found. The reduced transition probabilities  $B(E1, 599.5 \text{ keV}) = 1.3^{(+6)}_{(-4)} \times 10^{-6}$  W.u. and  $B(E1, 86.1 \text{ keV}) = 1.7^{(+7)}_{(-4)} \times 10^{-4}$  W.u. fit to the range of experimentally observed  $B(E1)$ -values given in the systematics [51].

A state with  $J^\pi = 25/2^+$  in  $^{113}\text{Sn}$  cannot be explained within the restricted shell-model space discussed in Sect. 3. Considering the excitations found in the even-mass neighbours  $^{112}\text{Sn}$  and  $^{114}\text{Sn}$ , a  $25/2^+$  state in  $^{113}\text{Sn}$  could arise either from a coupling of a  $2d_{5/2}$  or  $1g_{7/2}$  neutron ( $\nu$ ) to the proton 2p2h intruder band which starts with the  $0^+$  band head [15], or from a coupling of the same particles to  $\nu h_{11/2}^2$  states in  $^{112}\text{Sn}$  [16] or  $^{114}\text{Sn}$  [17]. Discussing the first case, only the coupling of a  $2d_{5/2}$  neutron to the  $0^+$  band head of the proton 2p2h band with  $\Delta J=2$  would result in a  $25/2^+$  member of the corresponding rotational band, whereas the corresponding coupling of an  $1g_{7/2}$  neutron would give  $J^\pi = 23/2^+$  or  $27/2^+$ . But, considering  $E_x = 4819$  keV of the  $10^+$  state of the proton 2p2h band in  $^{112}\text{Sn}$  [15, 16] and  $E_x = 410$  keV for the  $2d_{5/2}$  state in  $^{113}\text{Sn}$ , the  $25/2^+$  band member would have an excitation energy of about 5 MeV which is about 1 MeV above the experimental observation.

Therefore, in the following the coupling to  $\nu(h_{11/2}^2)$  is discussed. Thereby the energy of the  $25/2^+$  state is estimated with the mass formula formalism [52] for the two configurations  $\nu(h_{11/2}^2 d_{5/2}^{-1})$  with  $J = J_{max}$  and  $\nu(h_{11/2}^2 g_{7/2}^{-1})$  with  $J = J_{max}-1$ . Considering the behaviour of the energies  $E_x = 4680$  keV and 4140 keV for  $\nu h_{11/2}^2$  states in  $^{112,114}\text{Sn}$  [16, 17], respectively, and the dependence of the  $1g_{7/2}$ ,  $2d_{5/2}$  and  $1h_{11/2}$  neutron quasiparticle energies from the neutron number, these two configurations may be proposed for the  $25/2^+$  level in  $^{113}\text{Sn}$ . For the estimate,  $^{114}_{50}\text{Sn}_{64}$  has been assumed as magic core in analogy to  $^{146}_{64}\text{Gd}_{82}$  for the  $N = 82$  nuclei. This calculation results in  $E_x(\nu(h_{11/2}^2 g_{7/2}^{-1})) = 4054$  keV in surprisingly good agreement with the experiment. There are some reasons to favour this structure for the  $25/2^+$  state instead of the  $\nu(h_{11/2}^2 d_{5/2}^{-1})$  configuration: (i) The  $1g_{7/2}$  quasiparticle energy is lower than the  $2d_{5/2}$  energy, both in  $^{111}\text{Sn}$  and  $^{113}\text{Sn}$ ; (ii) Since neutron  $1h_{11/2}$  is mainly

particle-like while neutron  $1g_{7/2}$  and neutron  $2d_{5/2}$  are mainly hole-like, the particle-hole repulsion is strong for the maximally aligned  $\nu(h_{11/2}^2 d_{5/2}^{-1})$  configuration but much weaker for the  $\nu(h_{11/2}^2 g_{7/2}^{-1})$   $25/2^+$  structure. Generally, the  $N = 64$  shell closure of  $^{114}\text{Sn}$  is regarded as a poorer one than the  $Z = 64$  closure in  $^{146}\text{Gd}$ . Possibly, the very good agreement of the theoretical estimate with the experiment, assuming the magic character of  $^{114}\text{Sn}$ , is caused by the dominating influence of the unique parity neutron  $1h_{11/2}$  intruder state.

## 5 The odd-mass valence mirror nuclei $^{113}_{50}\text{Sn}_{63}$ and $^{145}_{63}\text{Eu}_{82}$

Assuming  $^{113}\text{Sn}$  and  $^{145}\text{Eu}$  as semi magic nuclei with closed  $N = 50$ ,  $Z = 50$  or  $Z = 50$ ,  $N = 82$  cores, respectively, the 13 active neutrons or protons should occupy the same shell model orbits. Such pairs of nuclei are denoted as quasimirror nuclei [13] or valence mirror nuclei [35–37]. As a consequence of the charge symmetry and charge independence of the nuclear forces, shell-model calculations for both nuclei using the same single-particle energies and the same residual interaction give identical results. But, for real calculations different shell-model parameters for tin nuclei and  $N = 82$  nuclei have to be used to obtain optimal correspondence between theory and experiment (cf. the corresponding table in [13]).

In Fig. 7 the experimentally observed yrast states of  $^{113}\text{Sn}$  are compared with the corresponding states in  $^{145}\text{Eu}$ . Like in the hitherto compared pairs of even-even valence mirror nuclei in this region, remarkable similarities are observed. The negative-parity states with  $11/2^- < J^\pi \leq 23/2^-$  have nearly the same level sequence and within 250 keV similar excitation energies. In both nuclei  $25/2^+$  and  $27/2^+$  states are found at nearly the same energy which should have  $1h_{11/2}^2$  components. Furtheron, in both nuclei no comparable positive-parity states with  $7/2^+ < J^\pi < 25/2^+$  are observed. For the  $1/2^+$ ,  $3/2^+$  and  $5/2^+$  states characterized by the occupation of the  $3s_{1/2}$ ,  $2d_{3/2}$  and  $2d_{5/2}$  shell model states large differences are found. On the other hand, the  $11/2^-$  states based on the  $1h_{11/2}$  orbit agree very well.

The observed similarities seem to be in contradiction to the different shell-model parameters used for the tin and  $N = 82$  nuclei. To explain this discrepancy, the influence of the extra neutron core between  $N = 50$  and  $82$  in the  $N = 82$  nuclei has to be considered [36]. As discussed in [36] the monopole proton-neutron residual interaction, e.g., is most attractive for the orbits proton  $1g_{9/2}$  and neutron  $1g_{7/2}$  causing a different behaviour of the  $g_{7/2} - d_{5/2}$  splitting in tin and  $N = 82$  nuclei. Thus, even if the underlying single-particle energies are different, the mirror similarity can persist. The comparison of  $^{113}\text{Sn}$  and  $^{145}\text{Eu}$  confirms the difficulty of the assumption of neutron-proton symmetry in the valence mirror nuclei.

## 6 Nearest-neighbour spacing distribution of the experimentally observed $5/2^+$ states

Shriner et al. [54] analyzed the fluctation properties of a large collection of low-lying nuclear energy levels in 60 nuclei with mass numbers  $24 \leq A \leq 244$  with emphasis on the nearest-neighbour spacing distributions. The aim of this study is to test the conjecture of Bohigas et al. [55] that for time-reversal invariant quantum systems the behaviour of fluctuation properties like a Gaussian orthogonal ensemble (GOE) is connected with chaoticity, and the behaviour as Poisson distribution with regularity.

As shown in Fig. 4, for  $E_x < 3$  MeV the number of experimentally observed positive parity states corresponds nearly to the number of theoretical predicted states with  $3/2^+ \leq J^\pi \leq 7/2^+$ , assuming the shell-model configuration space discussed in Subject 3.1. Especially



for  $J^\pi = 5/2^+$ , ten states have been identified and additional five levels with possible assignment  $5/2^+$  have been found. For two sequences of  $5/2^+$  states the nearest-neighbour spacing distributions are shown in Fig. 8. The probability density functions  $P(x)$  and the spacings  $x$  are obtained as described in [38], where  $^{116}\text{Sn}$  has been analyzed:  $x_i = S_i/D$ , where  $S_i$  are the spacings  $E_{i+1} - E_i$  of adjacent energy levels and  $D$  is the average of  $S_i$ . As found [38] for  $^{116}\text{Sn}$ , also here the two experimentally obtained nearest-neighbour spacing distributions show a behaviour between a Poisson- or GOE-distribution, i.e. the distinction between regular or chaotic behaviour is not possible. As stated in [56] shell-model states follow a GOE-distribution. On the other hand, with increasing mass number the fluctuation properties even in spherical nuclei seem to behave more and more like a Poisson distribution. Possibly the observed situation for the analyzed states in  $^{113}\text{Sn}$  reflects both tendencies.

## 7 Conclusions

On the basis of the comparison of the rich experimental data obtained in this work for  $^{113}\text{Sn}$ , with shell-model calculations the following conclusions can be drawn:

- (i) the experimentally observed level density of positive- and negative-parity states is approximately reproduced by the calculations, whereas the comparison of the experimentally determined electromagnetic properties of yrast states with the theoretical predictions shows large discrepancies.
- (ii) the used configuration space of the shell-model calculations seems to be too strongly restricted, but even the large-scale shell-model calculations for tin nuclei using only neutron excitations give no general improvement for the observed differences of experimental and calculated excitation energies.
- (iii) the consideration of the break-up of the  $Z = 50$  proton core, i.e. shell-model calculations allowing the excitations of both neutrons and protons, is supposed to give better results. The corresponding inclusion of the break-up of the  $N = 50$  neutron core in shell-model calculations for the  $N = 50$  nuclei  $^{86}_{36}\text{Kr}_{50}$  [57] and  $^{89}_{39}\text{Y}_{50}$  [58], e.g., results in a much better agreement between experiment and theory of both the energy levels and the electromagnetic properties. Because of the large configuration spaces for shell-model calculations of tin nuclei with neutron and proton excitations, sophisticated restrictions for the allowed occupations of the shell-model orbits have to be found.

During the preparation of the manuscript, we learned about preliminary data [59] of high-spin states in  $^{113}\text{Sn}$ . There, collective structures have been observed above the  $19/2^-$  state at 3093 keV. Thus,  $^{113}\text{Sn}$  once more is an example for the coexistence of different nuclear excitation modes and it is a challenge for the nuclear structure theory to describe this variety in one nucleus in a consistent way.

## Acknowledgements

We would like to thank Mrs. J. Kerber, Mrs. A. Uhlman and Mr. W. Schulze for the technical assistance during the experiments and preparation of the manuscript.

## References

- [1] M. Schimmer, S. Albers, A. Dewald, A. Gelberg, R. Wirowski and P.von Brentano, Nucl. Phys. A539(1992)527
- [2] R. Wadsworth, H.R. Andrews, R.M. Clark, D.B. Fossan, A. Galindo-Uribarri, J.R. Hughes, V.P. Janzen, D.R. LaFosse, S.M. Mullins, E.S. Paul, D.C. Radford, H. Schnare, P. Vaska, D. Ward, J.N. Wilson and R. Wyss, Nucl. Phys. A559(1993)461
- [3] R. Wadsworth, H.R. Andrews, C.W. Beausang, R.M. Clark, J. DeGraaf, D.B. Fossan, A. Galindo-Uribarri, I.M. Hibbert, K. Hauschild, J. R. Hughes, V.P. Janzen, D.C. Radford, H. Schnare, P. Vaska, D. Ward, J.N. Wilson and I. Ragnarsson, Phys. Rev. C50(1994)483
- [4] R. Schubart, D. Alber, R. Alfier, C. Bach, D.B. Fossan, H. Grawe, H. Kluge, K.H. Maier, M. Schramm, M. Waring and L. Wood, Z. Phys. A-Hadrons and Nuclei 340(1991)109
- [5] R. Schubart, H. Grawe, J. Heese, H. Kluge, K.H. Maier, M. Schramm, J. Grebosz, L. Käubler, H. Rotter, J. Kownacki and D. Seweryniak, Z. Phys. A-Hadrons and Nuclei 343(1992)123
- [6] T. Ishii, A. Makishina, K. Koganemarn, Y. Saito, M. Ogawa and M. Ischii, Z. Phys. A347(1993)41
- [7] H. Grawe, R. Schubart, D. Alber, D. Alfier, D.B. Fossan, J. Heese, H. Kluge, K.H. Maier and M. Schramm, Prog. Part. Nucl. Phys. 28(1992)281
- [8] Proc. of the Conf. SELMA94 "New Nuclear Structure Phenomena in the Vicinity of Closed Shells", Stockholm/Uppsala 1994, Physica Scripta, T56(1995)1
- [9] L. Käubler, H. Prade, J. Reif, R. Schwengner, G. Winter, H. Grawe, J. Heese, H. Kluge, K.-H. Maier, R. Schubart and K.-M. Spohr, Z. Phys. A351(1995)123
- [10] G. Gangopadhyay, A.K. Singh, D. Banerjee, R. Bhattacharya, R.K. Bhowmik, S. Muralithar, G. Rodrigueus, R.P. Singh, A. Goswami, S. Bhattacharya, B. Dasmahapatra and S. Sen, Z. Phys. A351(1995)1
- [11] O. Hashimoto, Y. Shida, G.Ch. Madueme, H. Yoshikawa, M. Sakai and S. Ohya, Nucl. Phys. A318(1979)145
- [12] A. van Poelgeest, J. Bron, W.H.A. Hesselink, K. Allaart, J.J.A. Zalmstra, M.J. Uitzinger and H. Verheul, Nucl. Phys. A346(1980)70
- [13] H. Prade, W. Enghardt, W.D. Fromm, H.U. Jäger, L. Käubler, H.-J. Keller, L.K. Kostov, F. Stary, G. Winkler and L. Westerberg, Nucl. Phys. A425(1984)317
- [14] W. Andrejtscheff, L.K. Kostov, P. Petkov, Y.Sy. Savane, Ch. Stoyanov, P. von Brentano, J. Eberth, R. Reinhardt and K.O. Zell, Nucl. Phys. A505(1989)397
- [15] J.Bron, W.H.A. Hesselink, A. van Poelgast, J.J.A. Zalustra, M.J. Uitzinger, H. Verheul, K. Heyde, M. Waroquier, H. Vincx and P. van Isacker, Nucl. Phys. A318(1979)335
- [16] H. Harada, T. Murakami, K. Yoshida, J. Kasagi, T. Inamura and T. Kubo, Phys. Lett. B207(1988)17
- [17] H.Harada, M. Sugawasa, H. Kusakari, H. Shinohara, Y. Ono, K. Furuno, T. Hosoda, M. Adachi, S. Matsuki, N. Kawamuri, Phys. Rev. C39(1989)132

- [18] F. Azaiez, S. Andriamonje, J.F. Chemin, M. Fidah, J.N. Scheurer, M.M. Aleonard, G. Bastin, J.P. Thiband, F. Beck, G. Costa, J.F. Bruandet and F. Liatard, Nucl. Phys. A501(1989)401
- [19] D.A. Viggars, H.W. Taylor, B. Singh and J.C. Waddington, Phys. Rev. C36(1987)1006
- [20] I.N. Vishnevsky, Yu. A. Dei, Yu. N. Lobach, O.B. Melnikov, I.P. Tkachuk, V.V. Trishin and T.V. Chaplitskaja, Conf. on Nucl. Spectroscopy and Nucl. Structure (in Russian), Charkov 1986, Nauka Leningrad 1986, p.90
- [21] I.N. Vishnevsky, Yu.A. Dei, Yu.N. Lobach, O.B. Melnikov, B.A. Sidorenko, I.P. Tkachuk, V.V. Trishin and Chaplitskaja, Abstract of the XXXVI. Conf. on Nucl. Spectroscopy and Nucl. Structure (in Russian), Charkov 1986, Nauka Leningrad 1986, p.91
- [22] I.N. Vishnevsky, Yu. A. Dei, Yu. N. Lobach, O.B. Melnikov, I.P. Tkachuk, V.V. Trishin and T.V. Chaplitskaja, Preprint KIJ-86-25(1961)1
- [23] L. Käubler, W. Enghardt, P. Kleinwächter and H. Prade, Annual Report 1986, ZfK-621(1987)36
- [24] I.N. Vishnevsky, Yu.A. Dei, Yu.N. Lobach, O.B. Melnikov, I.P. Tkachuk, V.V. Trishin and Chaplitskaja, Isv. Akad. Nauk SSSR, Ser. Fiz. 51(1987)873
- [25] I.N. Vishnevsky, M.J. Kirichenko, M.F. Kudojarov, E.V. Kuzmin, Yu. N. Lobach, A.A. Pasternak and V.V. Trishin, Abstract of the XXXVIII. Conf. on Nucl. Spectroscopy and Nucl. Structure (in Russian), Baku 1988, Nauka Leningrad 1988, p.87
- [26] I.N. Vishnevsky, M.J. Kirichenko, Yu.N. Lobach, I.P. Tkachuk, V.V. Trishin, M.F. Kudojarov, E.V. Kuzmin, A.A. Pasternak, L. Käubler, J. Döring and H. Prade, Annual Report 1988, ZfK-667(1989)33
- [27] I.N. Vishnevsky, M.J. Kirichenko, M.F. Kudojarov, E.V. Kuzmin, Yu. N. Lobach, A.A. Pasternak, I.P. Tkachuk and V.V. Trishin, Isv. Akad. Nauk Kas. SSR, Ser. Fiz.-Mat. (1989)64
- [28] L. Käubler, J. Döring, H. Prade, I.N. Vishnevsky, M.J. Kirichenko, Yu.N. Lobach, I.P. Tkachuk, V.V. Trishin, M.F. Kudojarov, E.V. Kuzmin, A.A. Pasternak, J. Blomqvist and L. Kostova, Book of Abstract of the Int. Conf. on High-Spin Physics and Gamma-Soft Nuclei, Pittsburgh, USA, Sept. 1990, p.90
- [29] L. Käubler and H. Prade, Verh. DPG1(1992)171
- [30] L. Käubler, J. Döring, P. Kleinwächter, H. Prade, I.N. Vishnevsky, M.J. Kirichenko, Yu.N. Lobach, I.P. Tkachuk, V.V. Trishin, M.F. Kudojarov, E.V. Kuzmin, A.A. Pasternak, J. Blomqvist and L. Kostova, Book of Abstract of the Nucl. Phys. Conf. Wiesbaden, Aug. 1992, p.1.2.16
- [31] L. Käubler, J. Döring, P. Kleinwächter, H. Prade, J. Reif, I.N. Vishnevsky, M.J. Kirichenko, Yu.N. Lobach, I.P. Tkachuk, V.V. Trishin, M.F. Kudojarov, E.V. Kuzmin, A.A. Pasternak, J. Blomqvist and L. Kostova, Poster at the Int. Phys. Conf. Wiesbaden, Aug. 1992
- [32] L. Käubler, J. Döring, P. Kleinwächter, H. Prade, I.N. Vishnevsky, M.J. Kirichenko, Yu.N. Lobach, I.P. Tkachuk, V.V. Trishin, M.F. Kudojarov, E.V. Kuzmin, A.A. Pasternak, J. Blomqvist and L. Kostova, Annual Report FZ Rossendorf, FZR 92-09(1992)34
- [33] J. Lyttkens, K. Nilson and L.P. Ekström, Nucl. Data Sheets 33(1981)1

- [34] J. Blachot, Nucl. Data Sheets 59(1990)729
- [35] R. Wirowski, J. Yan, P. von Brentano, A. Dewald and A. Gelberg, J. Phys. G. Nucl. Phys. 14(1988)L195
- [36] R.F. Casten, J. Yan, R. Wirowski, A. Gelberg, P. von Brentano and D.S. Brenner, Nucl. Phys. A514(1990)252
- [37] J. Yan, R. Wirowski, P. von Brentano, A. Dewald and A. Gelberg, Phys. Rev. C24(1990)743
- [38] S. Raman, T.A. Walkiewicz, S. Kahane, E.T. Journey, J. Sa, Z. Gácsi, J.L. Weil, K. Allaart, G. Bonsignori and F.F. Shriner, Jr., Phys. Rev. C43(1991)521
- [39] H. Prade, L. Käubler, U. Hagemann, H.U. Jäger, M. Kirchbach, L. Schneider, F. Stary, Z. Roller and V. Paar, Nucl. Phys. A333(1980)33
- [40] W. Andrejtscheff, F. Dubbers, P. Manfraß and K.D. Schilling, Nucl. Phys. A190(1972)489
- [41] K.D. Schilling, L. Käubler, F. Stary and W. Andrejtscheff, Nucl. Phys. A265(1976)58
- [42] P.C. Simnis, P. Anderson, F.A. Rickey, G. Smith, R.M. Steffen and J.R. Tesmen, Phys. Rev. C7(1973)1631
- [43] L. Käubler, H. Prade, J. Reif, R. Schwengner, G. Winter, H. Grawe, J. Heese, H. Kluge, K.-H. Maier, R. Schubart and K.-M. Spohr, Physica Scripta, T56(1995)266
- [44] T. Engeland, M. Hjorth-Jensen, A. Holt and E. Osnes, Physica Scripta T56(1995)58
- [45] N. Sandulescu, J. Blomqvist and R.J. Liotta, Nucl. Phys. A582(1995)257
- [46] W. Enghardt and H.U. Jäger, Nucl. Phys. A438(1985)141
- [47] D. de Frenne, E. Jacobs and M. Verboven, Nucl. Data Sheets 57(1989)443
- [48] M. Schimmer, R. Wirowski and P. von Brentano, Nucl. Phys. A587(1995)465
- [49] R.S. Hager and E.C. Seltzer, Nucl. Data Tables A4(1968)1
- [50] P. Raghavan, Atomic Data and Nucl. Data Tables 42(189)189
- [51] P.M. Endt, Atomic Data and Nuclear Data Tables 23(1979)547
- [52] J. Blomqvist, P. Kleinheinz and P.J. Daly, Z. Phys. A312(1983)27
- [53] L.K. Peker, Nucl. Data Sheets 68(1993)997
- [54] J. F. Shriner, Jr., G.E. Mitchel and T. von Egidy, Z. Phys. A 338 (1991)309
- [55] O. Bohigas, M.J. Giannoni and C. Schmit, Phys. Rev. Lett. 52 (1984) 1
- [56] T.A. Brody, J. Flores, J.B. French, P.A. Mello, A. Pandey and S.S.M. Wong, Rev. Mod. Phys. 53(1981)385
- [57] G. Winter, R. Schwengner, J. Reif, H. Prade, L. Funke, R. Wirowski, N. Nicolay, A. Dewald, P. von Brentano, H. Grawe and R. Schubart, Phys. Rev. C48(1993)1010
- [58] J. Reif, G. Winter, R. Schwengner, H. Prade and L. Käubler, Nucl. Phys. A587(1995)449
- [59] V. Janzen, private communication

## Figure captions

Fig. 1 Part of the level scheme of  $^{113}\text{Sn}$  obtained in this work showing the deexcitation of the observed negative-parity states and of high-spin positive-parity states. The experimentally observed mean lifetimes are given

Fig. 2 The low spin positive-parity states of  $^{113}\text{Sn}$  observed in this work. Experimentally deduced mean lifetimes are given

Fig. 3 Comparison of all low-spin positive parity-states (EXP) for  $^{113}\text{Sn}$ , observed experimentally in this work, with the results of our shell-model calculation (SMC). All calculated states with  $E_x < 4$  MeV are shown

Fig. 4 Comparison of all in this work experimentally observed and calculated positive-parity states with  $0.5 \text{ MeV} < E_x < 4.0 \text{ MeV}$  and  $3/2^+ \leq J^\pi \leq 7/2^+$ . The drawn calculated level scheme has been shifted down by 1010 keV to  $E_x^{exp}(5/2_2^+) = E_x^{th}(5/2_2^+)$

Fig. 5 Comparison of the experimentally identified negative-parity states in  $^{113}\text{Sn}$ , obtained in this work, with the result of our particle-core coupling (PCC) calculations. From the calculated states for  $9/2 \leq J \leq 27/2$  the first five levels are shown as long as  $E_x < 5.2$  MeV

Fig. 6 Comparison of some measured [47] yrast states in  $^{112}\text{Sn}$  with the results of shell-model calculations

Fig. 7 Comparison of experimentally observed yrast states in  $^{113}\text{Sn}$  with the corresponding levels in  $^{145}\text{Eu}$  [53]

Fig. 8 Nearest-neighbour spacing distributions for  $5/2^+$  levels in  $^{113}\text{Sn}$ : (i) the 10 levels with certain  $5/2^+$  assignment have been included (dashed line); (ii) 15 states with partly possible assignment  $5/2^+$  have been considered (solid line). Furtheron, a Poisson (dashed-dotted) and a GOE distribution (dots) is shown. For further explanation cf. the text

Table 1: Experimental data obtained in this work for  $\gamma$ -transitions and levels in  $^{113}\text{Sn}$

$E_\gamma(\text{keV})^a$	$I_{\gamma}(\%)^b$				$A_2^c$	$A_1^c$	$\delta_d^d$	$P_{\text{exp}}^e$	$P_f^d$	$\tau(\text{ps})^g$	$J_\pi^h$	$J_\pi^h$	$E_i(\text{keV})^h$
	(p,n)	( $\alpha$ ,n)	(p,3n)	( $\alpha$ ,2n)									
77.7										30.9min <sup>m</sup>	$7/2^+_{\text{m}}$	$1/2^+_{\text{m}}$	77.7
86.1					-0.13(1) <sup>f</sup>	-0.14(9) <sup>f</sup>					$25/2^+$	$(23/2^-)$	4059.1
87.8						-0.01(11) <sup>f</sup>					$3/2^+_{\text{m}}$	$5/2^+_{\text{m}}$	498.1
153.5					0.4(2)	0.4(2)					$3/2^+_{\text{m}}$	$(19/2^-)$	3129.9
172.4	1.7(1)	1.2(1)			0.15(5)	-0.04(6)					$7/2^+$	$5/2^+$	2040.0
225.3		0.5(2)	1.8(3)		0.10(2) <sup>f</sup>	0.09(3) <sup>f</sup>	0.25(5)	-0.61(51)	-0.28(15)		$7/2^+$	$17/2^-$	2976.0
282.7					0.5(2)						$(19/2^-)$	$11/2^-$	2620.1
291.7					1.8(2)						$21/2^-$	$21/2^-$	3421.1
322.5		1.1(1)	12(1)		0.01(4)	-0.03(5)		1.12(34)	0.39(4)	> 0.5	$21/2^-$	$19/2^-$	3129.9
329.5					5.8(5)	-0.01(7)		-0.68(23)	-0.45(349)		$23/2^-$	$21/2^-$	3459.5
332.6					-0.01(1)	-0.08(9)		-0.57(22)	0.12(126)		$5/2^+$	$21/2^-$	410.3
363.7	62(4)	44(3)	14(1)		-0.01(2)	0.01(2)	-0.08(2)				$5/2^+$	$7/2^+$	410.3
379.2					0.5(2)						$11/2^-$	$11/2^-$	2701.2
381.1					0.4(2)						$(23/2^-)$	$23/2^-$	3838.6
392.7					0.4(2)						$(11/2^-)$	$11/2^-$	2718.6
394.8					2.5(2)						$(19/2^-)$	$(15/2^-)$	2976.0
410.3					0.9(2)						$5/2^+$	$5/2^+$	1867.6
417.4					0.6(2)						$1/2^+$	$1/2^+$	410.3
498.1		0.3(1)			1.3(1)						$(27/2^+)$	$25/2^+$	4476.5
510.9 <sup>p</sup>	33(2)	30(2)	10(1)		0.38(13)	-0.11(14)	0.4(2)	-0.77(34)	-0.92(57)	> 0.5	$3/2^+$	$1/2^+$	498.1
518.4					0.13(4) <sup>f</sup>	0.06(5) <sup>f</sup>		0.2(1)	-0.68(29)				3131.1
543.5					-0.07(3)	-0.03(3)	0.12(6)	-0.14(14)	-0.22(12)				2386.0
551.9					0.09(8) <sup>f</sup>	0.02(11) <sup>f</sup>					$7/2^+$	$5/2^+$	2411.1
567.2					0.4(2)						$(23/2^-)$	$5/2^+$	3973.5
573.0	1.4(1)	1.2(1)			0.9(1)	0.12(10) <sup>f</sup>					$7/2^+$	$21/2^-$	2040.0
583.2	7.4(4)	7.1(4)			0.20(7)	0.12(8)					$5/2^+$	$5/2^+$	2045.8
599.5			5.6(7)		0.07(4) <sup>f</sup>	0.13(6) <sup>f</sup>					$(3/2^+_{\text{m}}, 5/2^+_{\text{m}})$	$5/2^+$	1867.6
608.0	38(3)	2.5(2)			8.0(4)	0.01(5)	0.15(10)	0.40(15)	0.22(8)	0.45(20)	$25/2^+$	$23/2^-$	4059.1
613.3					3.0(2)	0.04(2)		0.74(26)	-0.46(18) <sup>n</sup>	1000(400) <sup>+</sup>	$5/2^+$	$5/2^+$	1018.3
633.3	0.9(1)	1.2(1)			4.2(3)	0.06(3)	3(1)	0.83(76)	0.01(3)		$5/2^+$	$19/2^-$	3421.1
661.5 <sup>i</sup>	100(5)	100(4)	100(5)		0.7(2)	0.10(10) <sup>f</sup>	0.4(1)			0.10(5)	$21/2^-$	$15/2^-$	2540.9
678.7					1.0(1)	-0.06(15)	-1.2(8)	3459.5					
684.0					0.10(2)	-0.05(2)		-0.12(3)	0.13(4) <sup>o</sup>	124ns <sup>m</sup>	$11/2^-$	$7/2^+$	739.2
708.7					0.40(4) <sup>f</sup>	-0.05(4) <sup>f</sup>					$(23/2^-)$	$(19/2^-)$	3902.9
748.3					1.5(1)	-0.11(8) <sup>f</sup>					$7/2^+$	$3/2^+$	2040.0
755.8	0.8(1)	0.6(2)			-0.17(6) <sup>f</sup>	-0.11(8) <sup>f</sup>					$(23/2^-)$	$21/2^-$	3838.6
765.0					0.48(13) <sup>f</sup>	0.16(19) <sup>f</sup>					$13/2^-$	$13/2^-$	2701.2
					-0.13(11)	0.31(14)					$7/2^+$	$5/2^+$	2040.0
					0.4(2)						$11/2^-$	$11/2^-$	2701.2

Table 1: Experimental data obtained in this work for  $\gamma$ -transitions and levels in  $^{113}\text{Sn}$  (continuation)

$E_\gamma(\text{keV})^a$	(p,n) $E_p=6.7\text{MeV}$	( $\alpha$ ,n) $E_\alpha=18\text{MeV}$	(p,3n) $E_p=30\text{MeV}$	( $\alpha$ ,2n) $E_\alpha=27\text{MeV}$	$A_2^{\xi}$	$A_4^{\xi}$	$\delta_{ad}^d$	$P_{exp}^e$	$P_{ad}^f$	$\tau(\text{ps})^g$	$J_i^\pi$	$J_f^\pi$	$E_i(\text{keV})^h$
772.5				0.6(2)	-0.35(9) <sup>j</sup>	0.20(12) <sup>j</sup>	-3.0(15)				(11/2 <sup>-</sup> )	(9/2 <sup>-</sup> )	2718.6
786.0											5/2 <sup>+</sup>	5/2 <sup>+</sup>	2258.8
786.1	3.9(3)	4.4(2)	2.5(2)	2.8(2)	-0.14(1)	-0.02(2)		0.99(25)			5/2 <sup>+</sup>	3/2 <sup>+</sup>	1284.2
797.8		1.4(1)	3.0(3)	4.9(3)	0.30(4) <sup>j</sup>	-0.08(6) <sup>j</sup>		1.10(23)	0.56(13)	0.3(1)	17/2 <sup>-</sup>	13/2 <sup>-</sup>	2750.8
801.5	4.3(3)	3.6(3)	2.1(2)	2.0(2)	0.16(2)	-0.02(2)	-0.3(1)			0.35(10)	(11/2 <sup>-</sup> )	11/2 <sup>-</sup>	1540.7
808.0				0.5(2)								5/2 <sup>+</sup>	2675.6
810.1				1.8(2)							(23/2 <sup>-</sup> )	19/2 <sup>-</sup>	3902.9
812.0				0.7(1)	0.21(1)	-0.06(1)		0.69(34)			(27/2 <sup>-</sup> )	(23/2 <sup>-</sup> )	4714.9
838.4												9/2 <sup>-</sup>	2620.1
838.9	1.7(2)	2.3(2)		1.5(1)	0.06(4) <sup>j</sup>	0.08(6) <sup>j</sup>						5/2 <sup>-</sup>	1249.2
843.7				6.6(3)	0.14(5) <sup>j</sup>	0.15(12) <sup>j</sup>	0.25(5)				(23/2 <sup>-</sup> )	21/2 <sup>-</sup>	3973.5
873.9	2.3(1)	2.0(2)		0.6(2)	0.08(4)	0.04(5)	2.7(8)				5/2 <sup>+</sup>	5/2 <sup>+</sup>	1284.2
879.4	1.1(1)	1.1(1)		0.4(2)	0.03(3)	-0.06(3)						5/2 <sup>+</sup>	2624.6
892.6	3.3(2)	2.8(2)	2.2(2)	1.6(1)	-0.28(4)	0.01(5)	-0.2(1)			0.45(25)	7/2 <sup>+</sup>	5/2 <sup>+</sup>	2176.9
899.7											(17/2 <sup>-</sup> )	13/2 <sup>-</sup>	2852.7
900.1	2.0(2)	3.9(2)	14(2)	20.5(9)	0.31(4)	-0.10(5)		0.49(9)	0.50(9)	0.25(10)	19/2 <sup>-</sup>	15/2 <sup>-</sup>	2807.4
903.7	0.6(1)											3/2 <sup>+</sup>	1314.0
913.2	1.5(2)	1.8(1)		2.9(2)	0.19(5)	0.06(5)	0.4(2)				7/2 <sup>+</sup>	5/2 <sup>+</sup>	2386.0
936.7	4.5(3)	5.5(3)		1.6(1)	0.05(3)	-0.01(3)					3/2 <sup>+</sup>	7/2 <sup>+</sup>	1014.4
940.6	12.6(6)	12.0(6)	3.5(4)	2.5(2)	-0.25(4)	-0.02(5)	0.5(2)				5/2 <sup>+</sup>	7/2 <sup>+</sup>	1018.3
945.0				1.6(2)	0.48(18) <sup>j</sup>	0.34(21) <sup>j</sup>					(17/2 <sup>-</sup> )	15/2 <sup>-</sup>	2852.7
963.8				1.2(2)	-0.04(4) <sup>j</sup>	0.12(6) <sup>j</sup>						13/2 <sup>-</sup>	2916.8
974.6				1.2(1)							5/2 <sup>+</sup>	5/2 <sup>+</sup>	2258.8
975.8	1.0(1)	1.1(1)		1.9(1)	-0.24(6) <sup>j</sup>	-0.06(8)					7/2 <sup>+</sup>	5/2 <sup>+</sup>	2448.6
1009.1				0.2(1)								15/2 <sup>-</sup>	2916.8
1014.4	16(6)	3.6(2)		1.5(1)	0.10(2)	-0.02(3)	0.5(1)			0.3(1)	3/2 <sup>+</sup>	1/2 <sup>+</sup>	1014.4
1018.3	2.8(1)	2.5(2)	0.9(3)	0.3(2)	0.20(3)	-0.04(3)				1.4(7)	5/2 <sup>+</sup>	1/2 <sup>+</sup>	1018.3
1034.0				0.6(2)								5/2 <sup>+</sup>	2506
1042.3	8.0(4)	6.8(3)	3.8(4)	4.1(2)	0.26(4)	-0.02(5)	-0.5(3)			0.3(1)	9/2 <sup>-</sup>	11/2 <sup>-</sup>	1781.5

Table 1: Experimental data obtained in this work for  $\gamma$ -transitions and levels in  $^{113}\text{Sn}$  (continuation)

$E_\gamma(\text{keV})^a$	(p,n) $E_p=6.7\text{MeV}$	( $\alpha$ ,n) $E_\alpha=18\text{MeV}$	(p,3n) $E_p=30\text{MeV}$	( $\alpha$ ,2n) $E_\alpha=27\text{MeV}$	$A_2^c$	$A_4^c$	$\delta_{ad}^d$	$P_{esp}^e$	$P_{ad}^f$	$\tau(\text{ps})^g$	$J_i^\pi$	$J_f^\pi$	$E_i(\text{keV})^h$
1068.3		1.2(1)	2.0(2)	4.1(2)	0.31(5) <sup>j</sup>	-0.10(7) <sup>j</sup>		0.46(33)	0.50(12)	0.4(2)	(19/2 <sup>-</sup> )	15/2 <sup>-</sup>	2976.0
1079.8				0.3(2)								5/2 <sup>+</sup>	2552.6
1092.6				0.2(1)							7/2 <sup>+</sup>	3/2 <sup>+</sup>	2448.6
1101.8				0.4(2)							7/2 <sup>+</sup>	5/2 <sup>+</sup>	2386.0
1107.2				1.1(1)	-0.27(5) <sup>j</sup>	0.10(8) <sup>j</sup>					(21/2 <sup>-</sup> )	19/2 <sup>-</sup>	3914.6
1129.0	5.1(3)	4.4(3)	2.1(2)	1.2(2)	-0.16(2)	-0.04(2)	-2.5(10)			0.8(2)	5/2 <sup>+</sup>	5/2 <sup>+</sup>	1539.3
1147.2	2.6(1)	1.5(1)		0.3(2)								3/2 <sup>+</sup>	1645.3
1149.3				0.6(2)								3/2 <sup>+</sup>	1647.4
1151.8				0.1(1)								5/2 <sup>+</sup>	2624.6
1164.3	1.5(1)	1.2(1)	4.9(4)	2.9(2)	0.43(11)	0.15(12)	1.4(6)				7/2 <sup>+</sup>	5/2 <sup>+</sup>	2448.6
1168.3	8.8(6)	22.1(9)	35(2)	57(3)	0.30(1)	-0.08(1)		0.53(10)	0.49(3)	1.1(3)	15/2 <sup>-</sup>	11/2 <sup>-</sup>	1907.6
1185.1			2.5(2)	5.3(3)	0.25(3) <sup>j</sup>	-0.12(4) <sup>j</sup>		0.56(24)	0.36(7)		19/2 <sup>-</sup>	15/2 <sup>-</sup>	3092.8
1197.0	7.4(5)	7.3(4)	3.5(4)	3.3(2)	-0.24(1)	-0.18(1)	-5(3)			2.8(12)	11/2 <sup>-</sup>	11/2 <sup>-</sup>	1936.2
1202.8				0.6(2)	0.24(5) <sup>j</sup>	-0.15(20) <sup>j</sup>						5/2 <sup>+</sup>	2675.6
1206.9	3.5(3)	3.8(3)	2.6(2)	2.5(2)	-0.21(2)	-0.03(2)	0.15(5)			0.55(30)	(9/2 <sup>-</sup> )	11/2 <sup>-</sup>	1946.1
1213.6	8.1(4)	11.3(6)	8.4(7)	12.1(6)	0.32(2)	0.23(2)	3.4(2)	-0.46(13)	-0.11(3)	1.4(5)	13/2 <sup>-</sup>	11/2 <sup>-</sup>	1953.1
1221.6	1.0(1)	0.9(2)		0.9(1)	-0.26(4)	0.09(5)						5/2 <sup>+</sup>	2506
1223.6				0.4(2)								15/2 <sup>-</sup>	3131.1
1234.4	6.6(4)	3.8(3)		0.2(1)	0.30(1)	-0.01(1)					(3/2 <sup>+</sup> , 5/2 <sup>+</sup> )	3/2 <sup>+</sup>	1732.5
1237.1				0.2(1)								5/2 <sup>+</sup>	1647.4
1241.7	5.9(4)	4.0(3)		1.0(2)	-0.6(3)	0.1(4)					5/2 <sup>+</sup>	5/2 <sup>+</sup>	1652.1
1247.1	1.7(2)	1.4(1)		0.1(1)	0.26(5)	-0.04(6)	2.1(15)				5/2 <sup>+</sup>	3/2 <sup>+</sup>	1745.2
1268.4	0.3(1)			0.2(2)								5/2 <sup>+</sup>	2552.6
1271.6				0.4(2)								5/2 <sup>+</sup>	3139.2
1284.2	36(2)	28(2)	16(1)	12.5(6)	0.18(3)	-0.06(5)				0.7(3)	5/2 <sup>+</sup>	1/2 <sup>+</sup>	1284.2
1314.0	4.4(3)	5.0(3)	4.9(4)	2.6(2)	-0.11(2)	0.03(3)					3/2 <sup>+</sup>	1/2 <sup>+</sup>	1314.0
1316.5				2.4(2)	0.28(4) <sup>j</sup>	-0.05(5) <sup>j</sup>					(19/2 <sup>-</sup> )	15/2 <sup>-</sup>	3224.2
1334.9	11.8(6)	7.3(4)	3.1(3)	3.9(2)	0.26(5)	-0.04(6)	0.6(4)			0.4(1)	5/2 <sup>+</sup>	5/2 <sup>+</sup>	1745.2
1356.0	11(1)	8.8(4)	2.9(2)	2.2(2)	-0.04(3)	-0.03(4)	0.14(6)			1.0(5)	3/2 <sup>+</sup>	1/2 <sup>+</sup>	1356.0
1411.7	5.4(3)	3.7(3)	2.2(2)	1.2(2)	0.18(6)	0.02(7)					(5/2 <sup>+</sup> , 7/2 <sup>+</sup> )	3/2 <sup>+</sup>	1909.8
1472.8	24(2)	23.3(2)	15(1)	13.3(7)	0.22(6)	-0.07(6)		0.52(18)	0.33(12)	1.1(7)	5/2 <sup>+</sup>	1/2 <sup>+</sup>	1472.8
1499.5	4.5(2)	2.9(2)	2.5(2)	0.5(2)	0.11(6)	-0.04(7)					(5/2 <sup>+</sup> , 7/2 <sup>+</sup> )	5/2 <sup>+</sup>	1909.8
1502.8				0.6(2)	-0.44(6) <sup>j</sup>	0.02(8)						15/2 <sup>-</sup>	3410.5
1546.8												15/2 <sup>-</sup>	3454.5
1547.7	2.3(1)	2.0(2)	2.3(3)	1.9(1)	-0.036(3)	-0.02(3)							
1557.0	1.4(1)	1.4(1)	1.0(1)	0.7(2)	-0.04(2)	0.02(3)	0.2(1)				(3/2 <sup>+</sup> , 5/2 <sup>+</sup> )	3/2 <sup>+</sup>	2045.8
1574.5	4.1(3)	2.4(2)		0.5(2)	0.16(3)	0.09(4)	-1.0(5)				3/2 <sup>+</sup>	1/2 <sup>+</sup>	1557.0
1598.3	4.3(3)	4.0(3)	2.7(2)	2.2(2)	-0.21(1)	-0.12(3)	-1.9(2)			0.55(15)	5/2 <sup>+</sup>	7/2 <sup>+</sup>	1652.1
											11/2 <sup>-</sup>	11/2 <sup>-</sup>	2337.5



Table 1: Experimental data obtained in this work for  $\gamma$ -transitions and levels in  $^{113}\text{Sn}$  (continuation)

$E_\gamma(\text{keV})^a$	(p,n) $E_p=6.7\text{MeV}$	( $\alpha$ ,n) $E_\alpha=18\text{MeV}$	(p,3n) $E_p=30\text{MeV}$	( $\alpha$ ,2n) $E_\alpha=27\text{MeV}$	$A_2^c$	$A_4^c$	$\delta_{ad}^d$	$P_{exp}^e$	$P_{ad}^f$	$\tau(\text{ps})^g$	$J_i^\pi$	$J_f^\pi$	$E_i(\text{keV})^h$
1621.3	0.5(1)			0.1(1)								5/2 <sup>+</sup>	2031.6
1635.5	0.4(1)			0.1(1)							(3/2 <sup>+</sup> ,5/2 <sup>+</sup> )	5/2 <sup>+</sup>	2045.8
1667.5	4.8(3)	3.5(3)		1.2(1)	0.01(1)	-0.02(2)					5/2 <sup>+</sup>	7/2 <sup>+</sup>	1745.2
1672.4	0.6(1)	0.6(2)		0.3(1)								5/2 <sup>+</sup>	2956.6
1702.6	5.1(3)	3.9(3)	2.0(2)	1.3(1)	-0.33(6)	0.05(8)	-0.5(3)			>0.35	5/2 <sup>+</sup>	3/2 <sup>+</sup>	2200.7
1703.8				0.2(1)							9/2 <sup>-</sup>	7/2 <sup>+</sup>	1781.5
1725.1	1.4(1)			0.2(1)								5/2 <sup>+</sup>	2135.4
1766.5	0.4(1)			2.5(2)	0.15(5) <sup>j</sup>	0.02(6) <sup>j</sup>					7/2 <sup>+</sup>	5/2 <sup>+</sup>	2176.9
1801.6	1.2(1)	0.7(2)		1.1(1)	0.30(3)	-0.04(5)					(15/2 <sup>-</sup> )	11/2 <sup>-</sup>	2540.9
1821.0	0.1(1)											1/2 <sup>+</sup>	1821.0
1831.0	2.1(2)	1.4(1)										1/2 <sup>+</sup>	1831.0
1843.8	1.2(1)	2.4(2)	3.4(2)	3.7(2)	0.28(4) <sup>j</sup>	-0.09(6) <sup>j</sup>				0.2(1)	(15/2 <sup>-</sup> )	11/2 <sup>-</sup>	2583.2
1864.8	0.8(1)			0.1(1)								5/2 <sup>+</sup>	2275.1
1881.0				0.9(1)								11/2 <sup>-</sup>	2620.1
1910.6	1.2(3)	0.4(1)		0.2(1)	-0.4(2)	0.0(2)					(9/2 <sup>-</sup> )	11/2 <sup>-</sup>	2649.8
1932.7	0.7(1)	0.6(2)		0.1(1)								11/2 <sup>-</sup>	2671.9
1959.2	0.9(1)	1.1(1)										3/2 <sup>+</sup>	2457.3
1962.0				0.7(2)	0.20(8) <sup>j</sup>	-0.1(1) <sup>j</sup>						11/2 <sup>-</sup>	2701.2
1969.8	0.9(1)											3/2 <sup>+</sup>	2467.9
1979.4				0.6(2)	0.35(7) <sup>j</sup>	-0.17(10) <sup>j</sup>					(11/2 <sup>-</sup> )	11/2 <sup>-</sup>	2718.6
2013.9	2.5(2)	1.4(1)		0.5(2)	0.04(3)	0.09(4)					(3/2 <sup>+</sup> ,5/2 <sup>+</sup> )	3/2 <sup>+</sup>	2512.0
2039.5	3.6(4)	1.4(1)	1.4(3)	1.6(1)	0.28(4)	-0.04(5)						11/2 <sup>-</sup>	2778.7
2040.3	2.7(4)		1.0(3)									3/2 <sup>+</sup>	2538.5
2047.1	0.2(4)											5/2 <sup>+</sup>	2457.3
2092.9	0.1(1)	0.1(1)										3/2 <sup>+</sup>	2591.0
2099.3	1.4(1)	1.2(1)		1.4(1)	-0.32(7)	-0.06(7)					7/2 <sup>+</sup>	7/2 <sup>+</sup>	2176.9
2128.3	1.5(1)											5/2 <sup>+</sup>	2538.5
2150.5	1.8(1)	0.6(2)		0.2(1)								11/2 <sup>-</sup>	2889.7
2164.7	3.5(3)	1.3(1)	0.9(1)	0.9(3)	-0.29(6)	-0.09(7)					(3/2 <sup>+</sup> ,5/2 <sup>+</sup> )	3/2 <sup>+</sup>	2662.8
2180.7	0.9(1)											5/2 <sup>+</sup>	2591.0
2206.9	6.9(6)	0.3(1)	2.2(2)		-0.6(4)	0.4(4)						5/2 <sup>+</sup>	2617.2

<sup>a</sup> The errors of the energy values amount to (0.1 – 0.4) keV

<sup>b</sup> Relative  $\gamma$ -ray intensities

<sup>c</sup> Angular distribution coefficients measured in the ( $\alpha$ ,n) reaction or in the ( $\alpha$ ,2n) reaction (footnote<sup>j</sup>), cf. the text.

<sup>d</sup> Multipole mixing ratio obtained from the angular distribution data by including the attenuation

<sup>e</sup> Experimental  $\gamma$ -linear polarization

<sup>f</sup> Polarization calculated from  $A_2$ ,  $A_4$  and  $\delta$

<sup>g</sup> Mean lifetime of the deexciting state obtained with the DSA method or the  $\gamma$ -RF method (footnote<sup>k</sup>)

<sup>h</sup> The assignment of the transition in the level scheme indicated by the energy of the initial state

- i* Normalization
- j* ( $\alpha, 2n$ ) reaction
- k*  $\gamma$ -RF method
- l* Obtained by Hashimoto et al. [11] in the ( $\alpha, 3n$ ) reaction
- m* Taken from [34]
- n* For M1
- o* For E2
- p* Superimposed by a background line

Table 2: Comparison of some electromagnetic properties for yrast states in  $^{113}\text{Sn}$  obtained mainly in this work with predictions of our SMC or PCC calculations (cf. the text)

$J_i^\pi$	$J_f^\pi$	$\sigma L$	$E_\gamma^{exp}(\text{keV})$	electromagnetic property	
				exp	theory <sup>a</sup>
				$B(\sigma L)(\text{W. u.})^b$	
3/2 <sup>+</sup>	1/2 <sup>+</sup>	M1	498.1	<0.5 <sup>c</sup>	5.6×10 <sup>-6</sup>
		E2		<24	0.46
3/2 <sup>+</sup>	5/2 <sup>+</sup>	M1	87.8	<50 <sup>d</sup>	0.039
9/2 <sup>-</sup>	11/2 <sup>-</sup>	M1	1042.3	0.071 <sup>+0.036</sup> <sub>-0.018</sub>	4.5×10 <sup>-4</sup>
		E2		13 <sup>+6</sup> <sub>-3</sub>	0.51
11/2 <sup>-</sup>	7/2 <sup>+</sup>	M2	661.5	0.0156 <sup>+0.0004</sup> <sub>-0.0004</sub> <sup>e</sup>	0.068
		E3		290 <sup>+7</sup> <sub>-7</sub>	2.5×10 <sup>-9</sup>
13/2 <sup>-</sup>	11/2 <sup>-</sup>	M1	1213.6	0.0010 <sup>+0.0006</sup> <sub>-0.0006</sub>	0.0022
		E2		6.3 <sup>+3.5</sup> <sub>-1.7</sub>	0.75
15/2 <sup>-</sup>	11/2 <sup>-</sup>	E2	1168.3	11 <sup>+4</sup> <sub>-2</sub>	0.84
17/2 <sup>-</sup>	13/2 <sup>-</sup>	E2	797.8	260 <sup>+130</sup> <sub>-60</sub>	2.1×10 <sup>-4</sup>
19/2 <sup>-</sup>	15/2 <sup>-</sup>	E2	900.1	170 <sup>+110</sup> <sub>-50</sub>	0.089
21/2 <sup>-</sup>	19/2 <sup>-</sup>	M1	322.5	< 1.8	0.029
		E2		<300	0.86
				magnetic moment $\mu(\mu_N)$	
1/2 <sup>+</sup>				-0.8791(6) <sup>f</sup>	-1.13
11/2 <sup>-</sup>				-1.293(16) <sup>f</sup>	-1.11
				quadrupole moment Q(eb)	
11/2 <sup>-</sup>				±0.41(1) <sup>f</sup>	-0.39

<sup>a</sup> Electric properties have been calculated with  $e^{eff} = 0.442e$ , magnetic ones with  $g_s^{eff} = 0.6g_s^{free}$ .

<sup>b</sup> Reduced transition probability in Weisskopf units: 1 W.u.(M1) = 1.8  $\mu_N^2$  and 1 W.u.(E2) = 21.5 e<sup>2</sup>fm<sup>4</sup>. For the calculation of the experimental  $B(\sigma L)$  values, the mean lifetimes  $\tau$ , transition energies  $E_\gamma$  and mixing ratios  $\delta$  given in Table 1 have been used. The total conversion coefficients  $\alpha_{tot}$  have been taken from [49].

<sup>c</sup> The 87.8 keV transition has been neglected, since no intensity value is available

<sup>d</sup> Pure M1 transition assumed

<sup>e</sup>  $\delta$  and  $\alpha_{tot}$  taken from [33]

<sup>f</sup> Taken from [50]

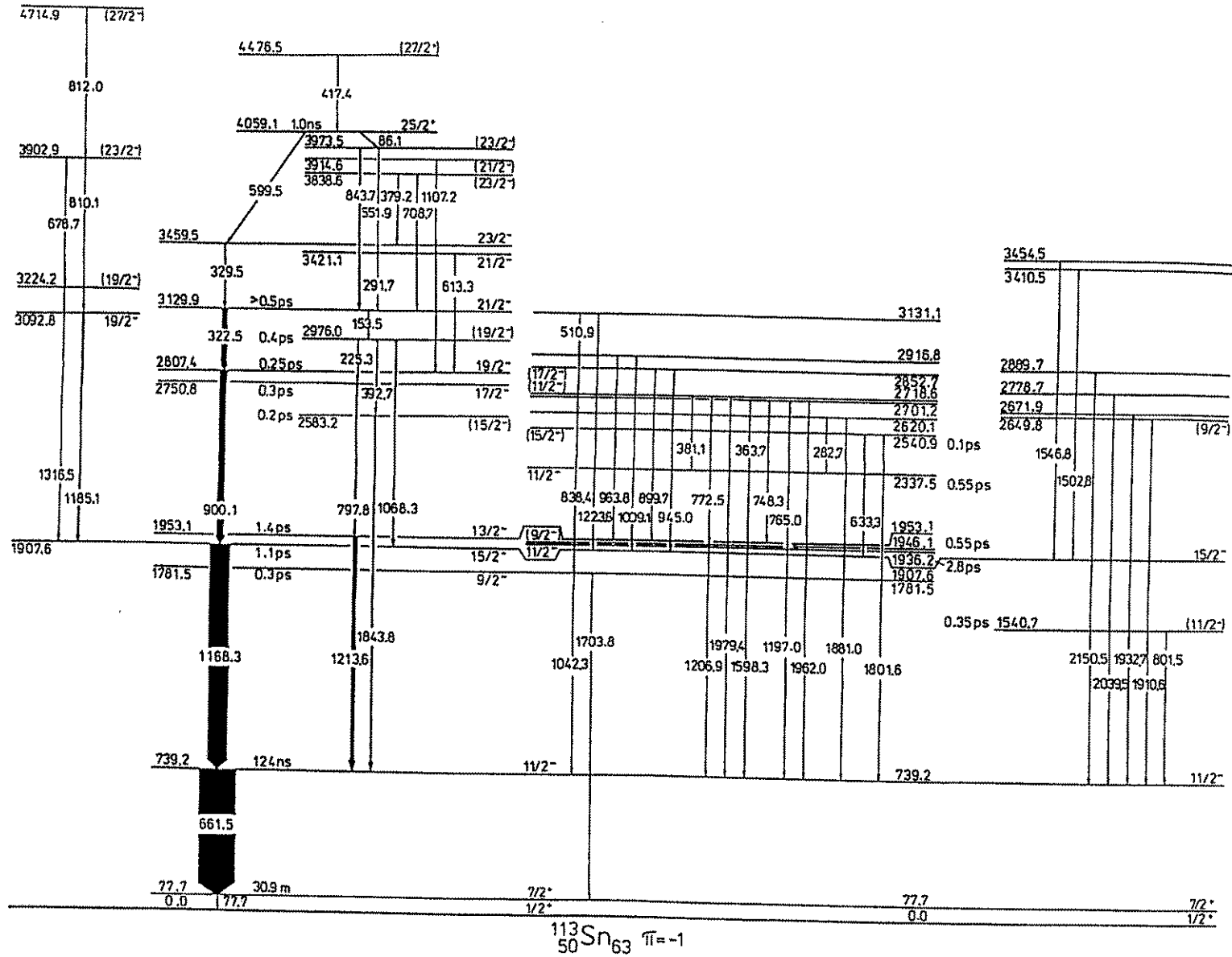
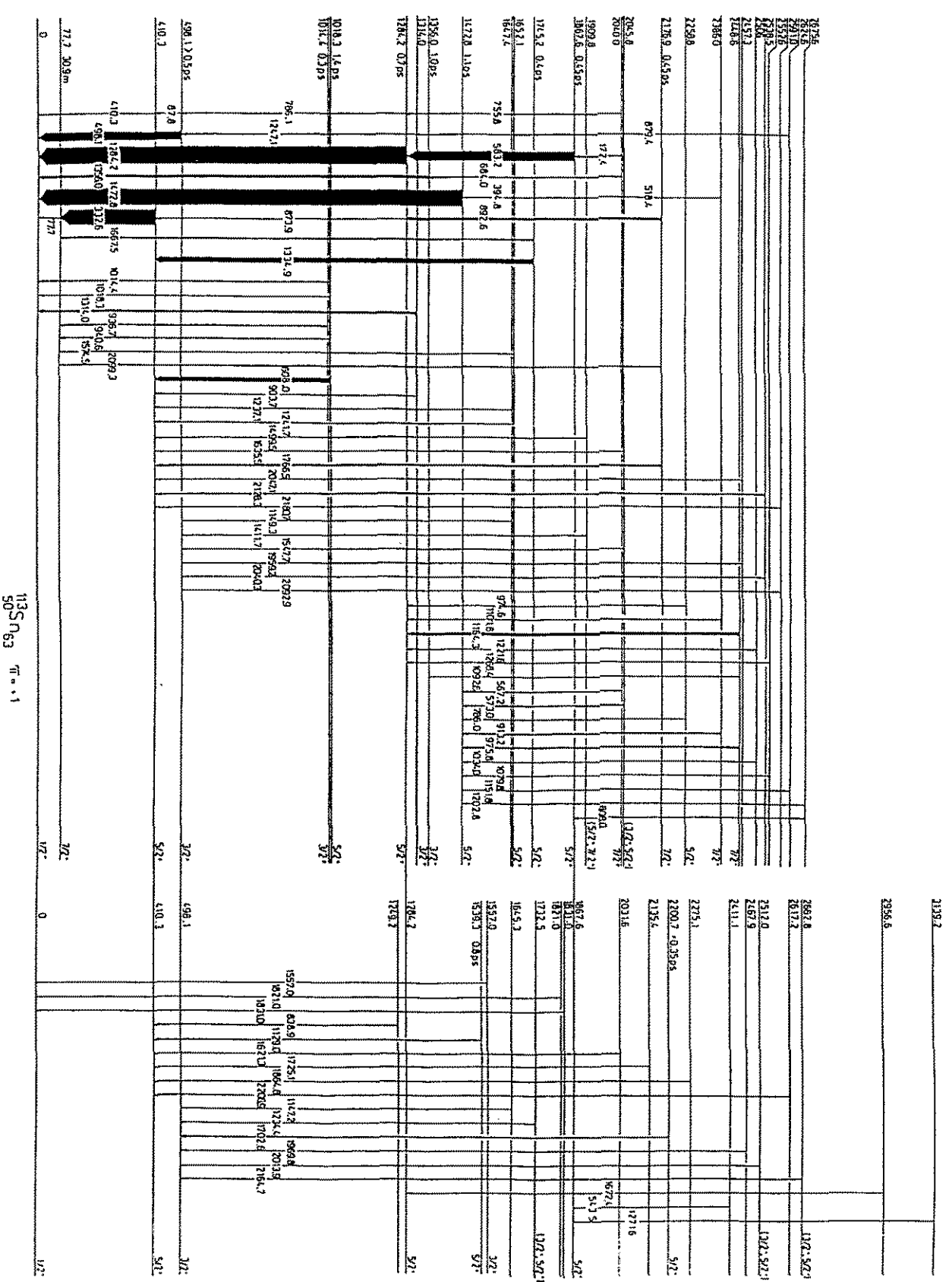


Fig.1



1135.0 1.095  
50° N 63 π = .1

Fig. 2

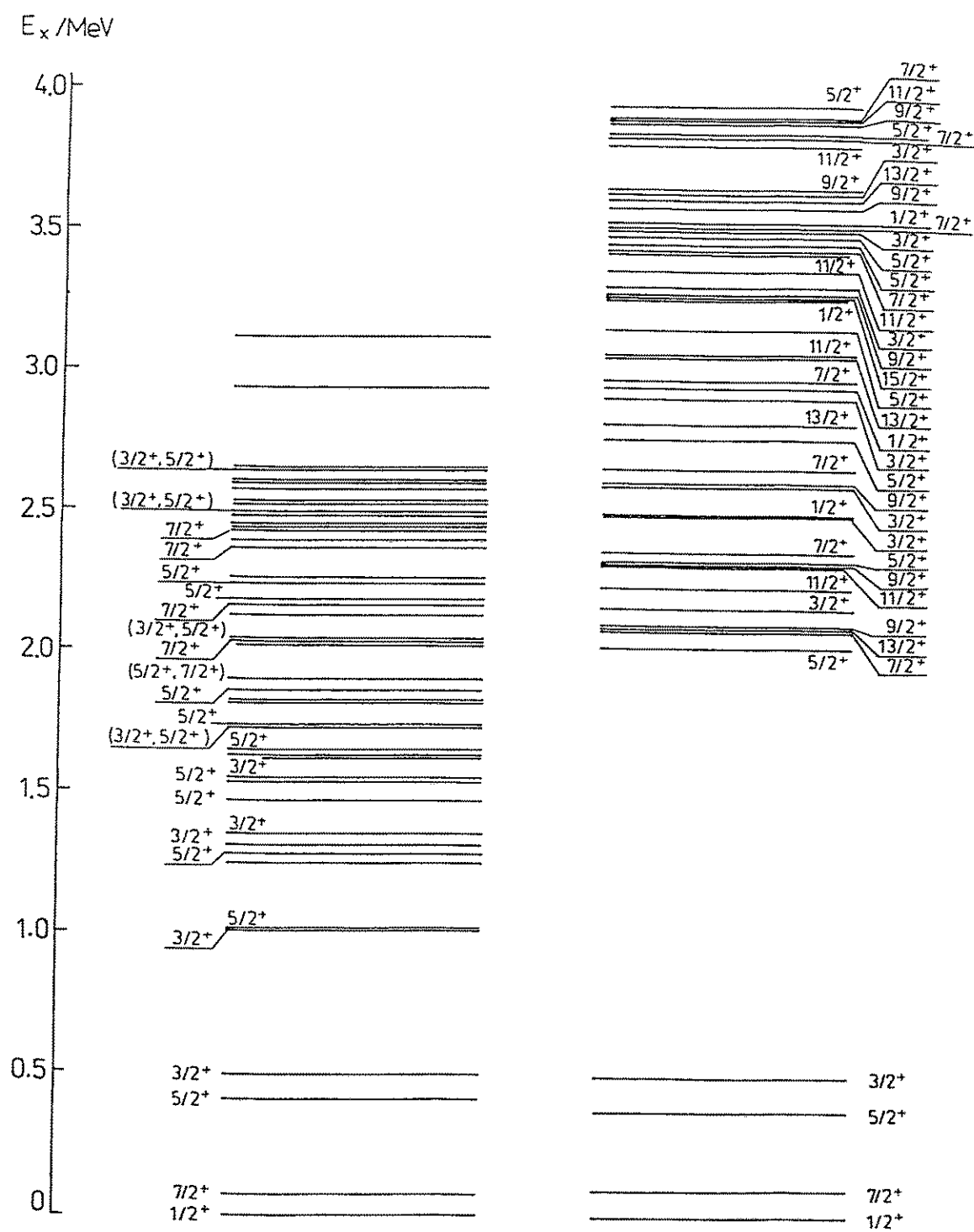


Fig.

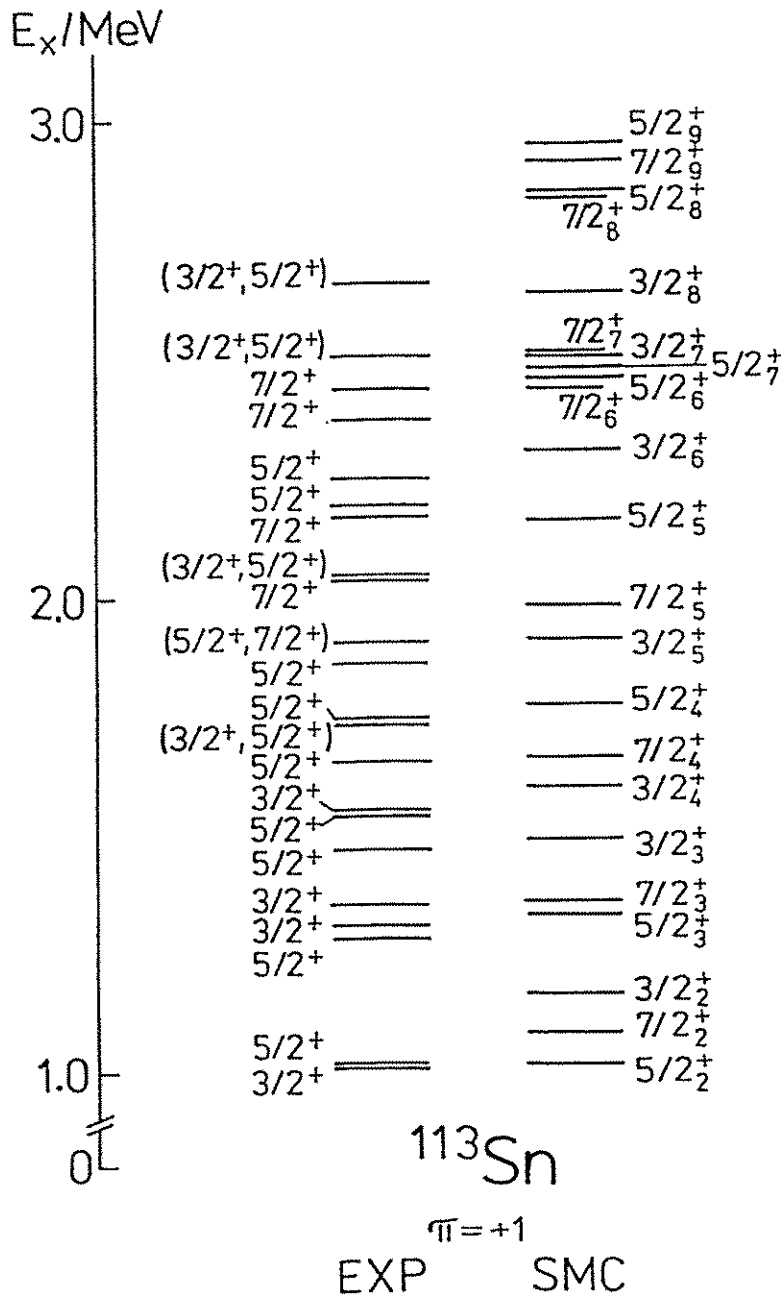


Fig.4

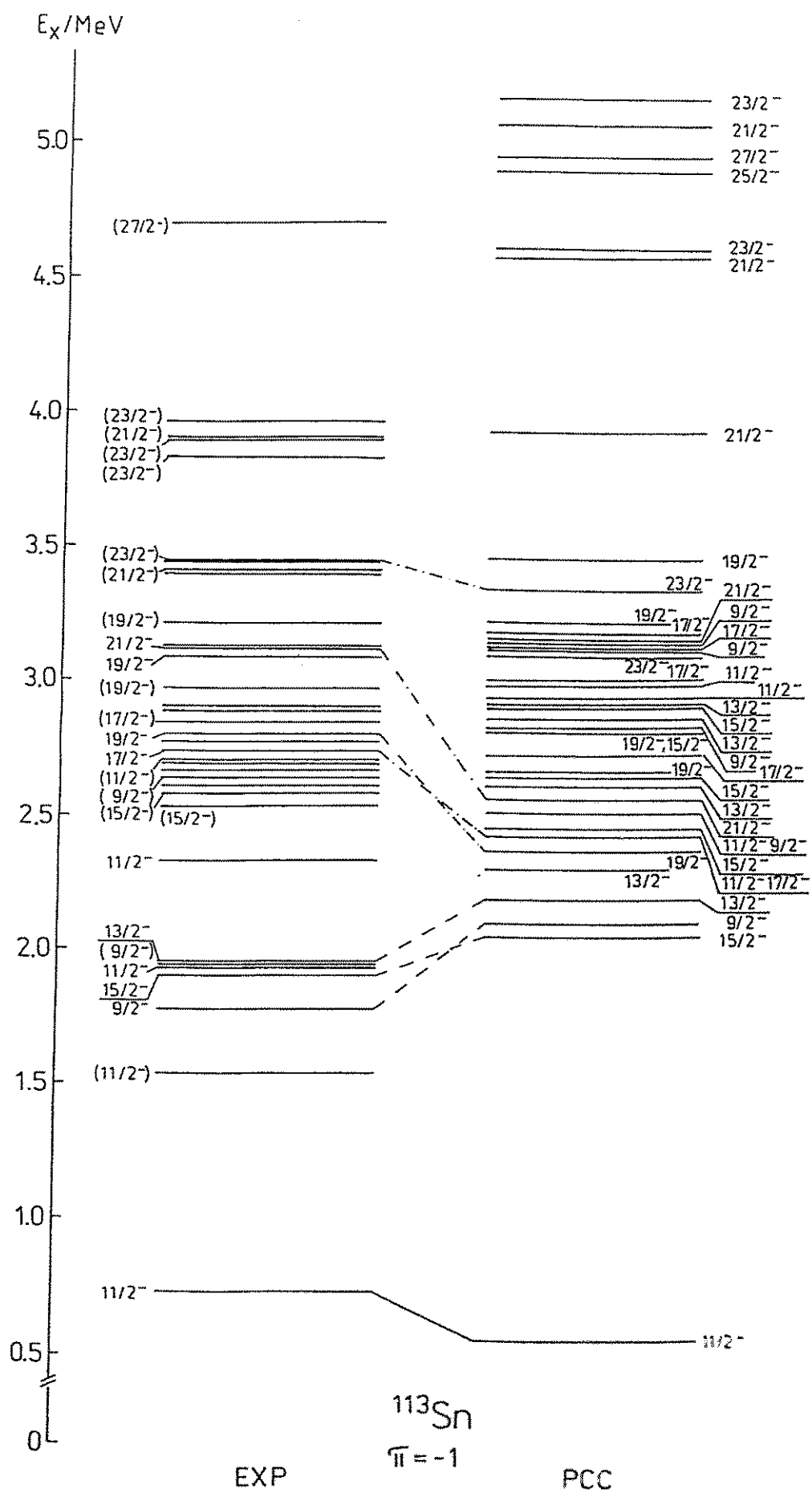


Fig.5



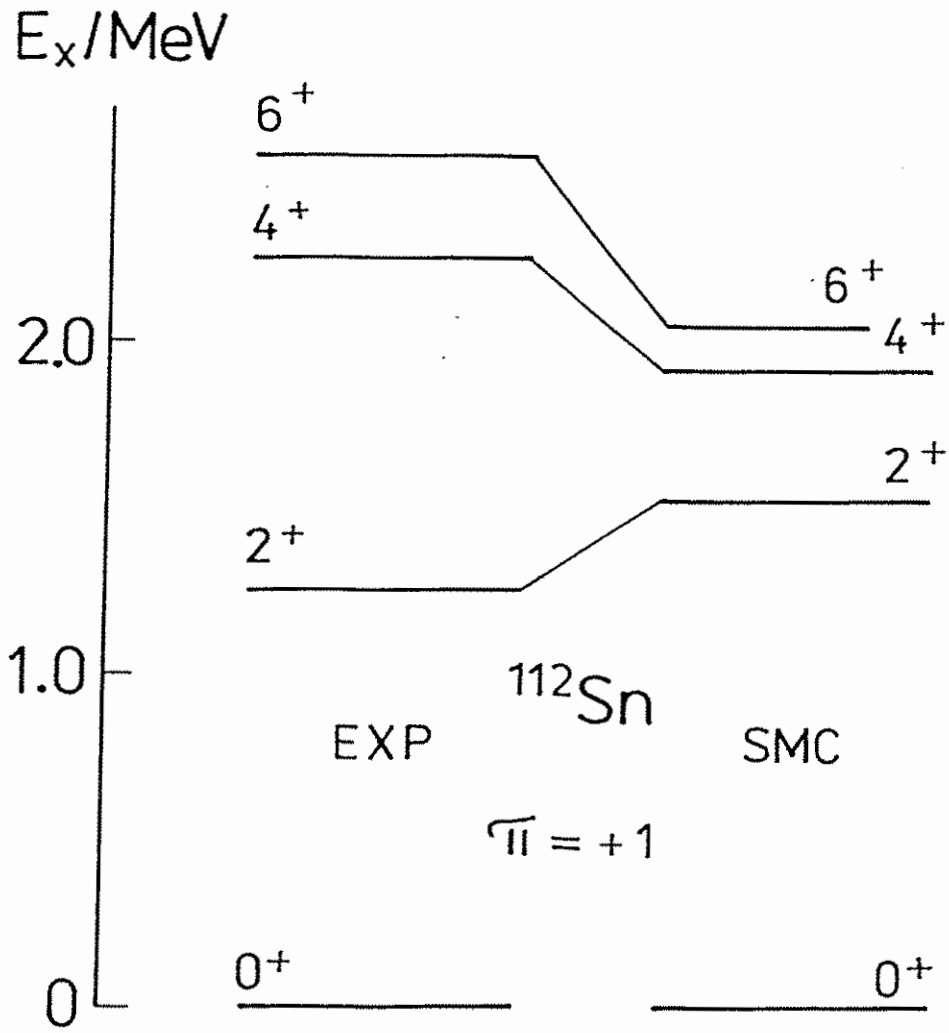


Fig.6

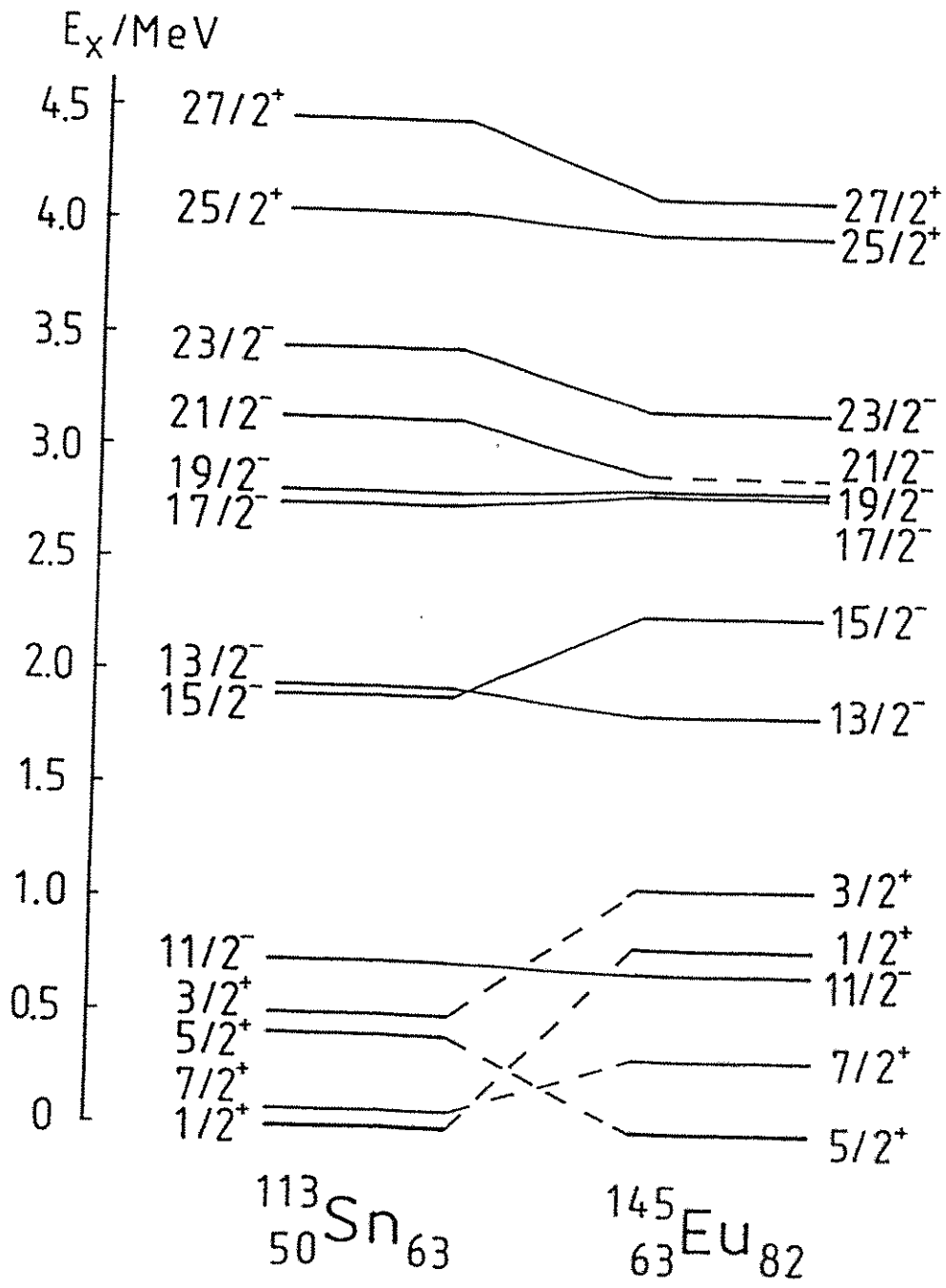


Fig.

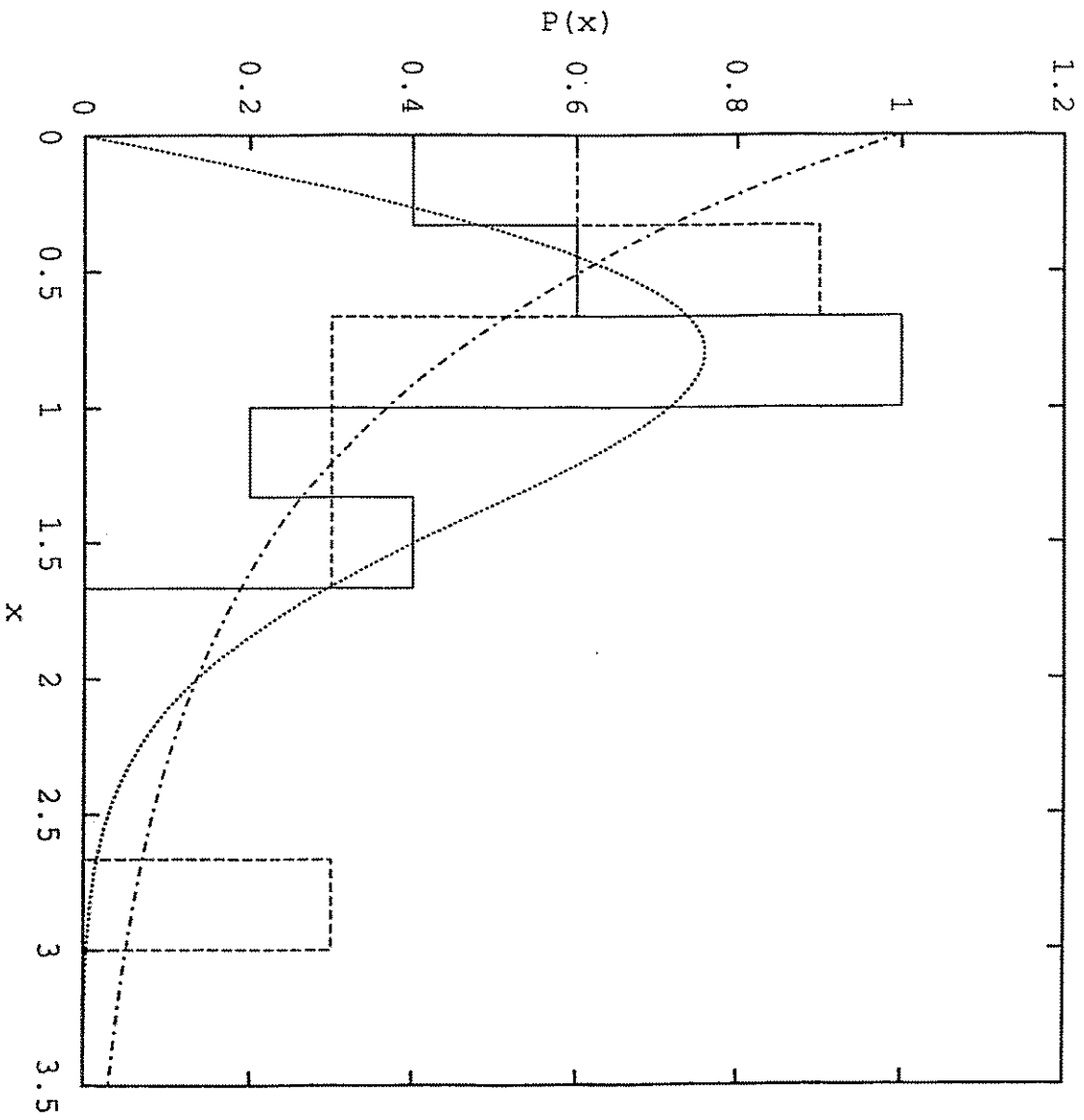


Fig. 8